Considering Wind Speed Characteristics in the Design of a Coreless AFPM Synchronous Generator

A. Daghigh*‡, H. Javadi*, H. Torkaman*

*Faculty of Electrical Engineering, Shahid Beheshti University, A. C., Tehran, Iran.

(a_daghigh@sbu.ac.ir, h_javadi@sbu.ac.ir, h_torkaman@sbu.ac.ir)

‡ Corresponding Author; A. Daghigh, Shahid Beheshti University, A.C., Hakimyeh St., East Vafadar Blvd., 4th Tehranpars sq., P.O.Box: 16765-1719, Tehran, Iran, Tel: (+9821) 73932529, Fax: (+9821) 77310425, a_daghigh@sbu.ac.ir

Received: 07.12.2015 Accepted:10.01.2016

Abstract- This paper presents an improved design procedure of a coreless Axial Flux Permanent Magnet Synchronous Generator (AFPMSG) for wind turbine application. An analytical design approach is proposed based on sizing equations and a nonlinear Magnetic Equivalent Circuit (MEC) model of AFPMSG. The reluctance of rotor back iron core is separated into two parts, which are calculated through the nonlinear iterative algorithm. An optimal design of the coreless AFPMSG is performed using Partial Swarm Optimization (PSO) method in order to increase the Annual Energy Yield (AEY) of the generator. The statistical model of wind speed distribution and wind turbine characteristic are used for considering the generator performance over the whole operating wind speed range. The proposed procedure is used to design a double rotor-one coreless stator AFPMSG. Finally, 3-D Finite Element Analysis (FEA) is used to validate the design algorithm. Also, the generator performance is evaluated for different values of wind speed and load currents.

Keywords Axial Flux Permanent Magnet Generator, coreless, design optimization, wind speed characteristics, finite element model.

1. Introduction

Recently, wind turbine technologies have been developed noticeably and the use of gearless systems is taken into consideration greatly [1]. Gearless systems have the advantages of lightweight, noise reduction and lower maintenance cost. AFPMSG with high ratio of generator diameter to generator length is one of the appropriate choices in gearless wind turbine applications [2]. According to the type of materials used in manufacturing of the stator cores, AFPMSGs are classified into two types: iron-cored and coreless generators [3]. Compared with iron-cored generators, coreless ones can start with low torque and operate with high efficiency. Absence of cogging torque in these machines helps the turbine starting [4]. Simple construction, negligible attraction force between the stator and the rotor, lightweight, no saturation in the stator structure, and low armature inductance are the other advantages of these machines [5, 6]. However, because of the large effective air gap length in the coreless machines, PM consumption is higher in comparison to iron-cored machines.

The design analysis and optimization of AFPM generators in wind turbine applications has received great attention in recent researches. An optimal design of a high speed coreless AFPMSG has been presented in [7] based on analytical and FE analysis. Chan et al. investigated the design and analysis of coreless AFPMSG with compatible structure to horizontal and axial axis wind turbines [8]. In [9], an optimal design of Radial Flux PM (RFPM) wind generator for maximum annual energy production has been provided through distributed parallel computing system via internet web service. The other design optimization of an iron-cored RFPM wind generator has been investigated in [10], without considering the design characteristics and constraints. Characteristic analysis of iron-cored AFPMSG for small scale wind turbine has been presented in [11] by considering wind turbine characteristics. In recent studies, improved design of iron-cored AFPM machines using Genetic Algorithm (GA) have been evaluated for the minimum material cost [12] and the maximum power density with low cogging torque [13]. Particle Swarm Optimization (PSO) of an coreless AFPMSG for small scale wind turbine application has been presented in [14], but the wind speed

characteristic has not been considered in the design procedure.

In an iterative design procedure of coreless AFPMSG, the stator axial length variation results in changing of the effective air gap length. Therefore, the value of Permanent Magnet Leakage Flux (PMLF) factor and PM axial length are changed. So, the precise prediction of leakage flux coefficient is very important in the case of coreless machines. The PMLF modelling for the iron-cored AFPM machines are investigated in [15, 16]. The leakage flux consideration in modelling of high speed coreless AFPMSG was presented in [17]. But, the analytical and FEM results of the PMLF model weren't provided well. An analytical design framework for coreless RFPM machines was presented in [18] according to the MEC model of the machine.

In this study, an optimal design of coreless AFPMSG is considered for wind turbine application. For considering the generator performance over whole operating wind speeds the value of output power and AEY is computed according to the wind speed distribution and turbine characteristics. The objective function is defined and implemented through the PSO algorithm to design a generator with high amount of AEY. For accurate calculation of the PMLF factor, a nonlinear MEC model of the coreless AFPMSG was presented with consideration of the rotor back iron reluctance. In the following, wind turbine characteristics are considered in Section 2. Analytical design equations are given in Section 3. Section 4 introduces the PSO based optimal design procedure. Finally, the improved design procedure is validated by 3-D FEA in Section 5.

2. Consideration of Wind Turbine and Wind Speed Characteristics

Consideration of wind turbine and wind speed characteristics is an important issue in the design of AFPM wind generators. Hence, in the design stage, beside the other design constraints and requirements, it is essential to consider the generator performance over the whole operating wind speed range. Accurate prediction of a wind turbine's power curve is an important step in the design process. It includes consideration of the turbine, generator, and control system. The output power of a wind turbine (P_{shaft}) can be expressed as follows [19];

$$P_{shaft} = 0.5\rho_{air} C_p(\lambda,\beta)\pi R_b^2 v_w^3 \quad (1)$$

where R_b is radius of the turbine blade, v_w is wind speed, ρ_{air} is air density, and $C_p(\lambda,\beta)$ is the power coefficient. To calculate $C_p(\lambda,\beta)$ for the given values of tip speed ratio (λ) and pitch angle (β), the following numerical approximation has been used in this study [20].

$$C_p(\lambda,\beta) = c_1\left(\frac{c_2}{\lambda_i} - c_3\beta - c_4\right)e^{\frac{-c_5}{\lambda_i}} + c_6\lambda \quad (2)$$

$$\frac{1}{\lambda_i} = \frac{1}{\lambda + 0.08\beta} - \frac{0.035}{\beta^3 + 1} \quad (3)$$

where c_1=0.5176, c_2=116, c_3=0.4, c_4=5, c_5=21, and c_6=0.0068. The tip speed ratio is defined as (4) [19];

$$\lambda = \frac{\omega_m R_b}{v_w} \quad (4)$$

The specifications of the wind turbine that is considered in this study, are given in Table 1. Its output power curves in relation to the rotational speed are shown in Fig. 1. It can be seen that, for any particular wind speed, there is a rotational speed that corresponds to the maximum power (P_{max}). When the wind speed changes, the rotational speed is controlled to follow the maximum power point trajectory. Below the rated speed of the generator, P_{max} is achieved for an optimum value of λ_{opt}, $C_{p\text{-}opt}$ and β=0, as follows; [21]

$$P_{max} = 0.5\rho_{air}\pi R_b^5 \omega_m^3 \frac{C_{p\text{-}opt}}{\lambda_{opt}^3} \quad (5)$$

In order to design a generator with considering the whole operating wind speed range, it is necessary to assume the wind speed distribution in addition to wind turbine characteristics. Rayleigh distribution, which is commonly used in wind data analysis, is considered to represent the wind resource. The probability density function $P(v_w)$ and the cumulative distribution function $F(v_w)$ are given by (6) and (7) [19].

Table 1. The specifications of the wind turbine

Parameter	Value
Rated rotational speed (n_m)	200 (rpm)
Rated wind speed (v_w)	11.5 (m/s)
Radius of the turbine blade (R_b)	4.8 (m)
Maximum power coefficient ($C_{p\text{-}max}$)	0.48
Air density (ρ_{air})	1.225 (kg/m^3)

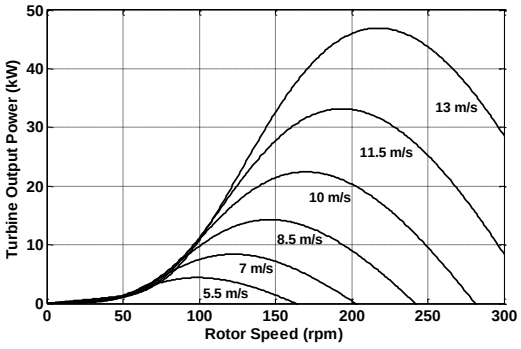

Fig. 1. Output power curves of the wind turbine

$$P(v_w) = \frac{\pi}{2}\left(\frac{v_w}{v_{av}^2}\right)\exp\left[-\frac{\pi}{4}\left(\frac{v_w}{v_{av}}\right)^2\right] \quad (6)$$

$$F(v_w) = 1 - \exp\left[-\frac{\pi}{4}\left(\frac{v_w}{v_{av}}\right)^2\right] \quad (7)$$

where v_{av} is the average wind speed. Figure 2 illustrates a Rayleigh probability density function for different mean wind speeds.

The AEY conception is considered in the design procedure of the coreless AFPMSG instead of computation of the output power and efficiency at a certain speed. The total amount of energy production covering the whole operating wind speed, can be calculated from (8) [9].

$$AEY = \sum P_{out}(v_w)H(v_w) \quad (8)$$

where $H(v_w)$ is the effective operating hour at the given wind speed and has been calculated using Rayleigh probability density function as follows;

$$H(v_w) = 8760\, P(v_w)\Delta v_w \quad (9)$$

3. Analytical Design

3.1. Main Design Equations

In this study, the proposed AFPMSG consists of two parallel rotors and one inner coreless stator. Trapezoidal permanent magnets are placed on the rotor surfaces and the concentrated winding coils of the stator are held together by using composite material of epoxy resin. A model of the coreless AFPMSG is shown in Fig. 3. The main dimensions of each electrical machine are determined by the electrical output power equation of the machine, as expressed in (10) for the AFPM machines [22].

$$P_{out} = \frac{\pi^3\sqrt{2}}{32}\alpha_i k_{w1} n_s D_{out}^{\ 3} B_g A_e (1+k_d)^2 (1-k_d)\eta\cos(\varphi) \quad (10)$$

where D_{out}, A_m, B_g, n_s, α_p, k_{w1}, and k_d are the outer diameter, maximum electrical loading, flux density of the air gap, rotational speed, magnet width to pole pitch ratio, winding factor, and the inner to outer diameter ratio, respectively. k_d is one of the important parameters in AFPMSG design, which has great influence on the performance of the generator [8, 23].

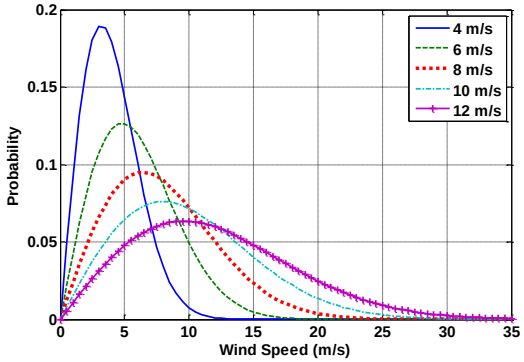

Fig. 2. Rayleigh probability density function

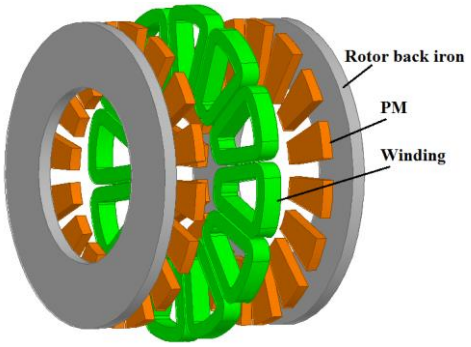

Fig. 3. Model of the coreless AFPMSG

Different configurations of concentrated winding for the coreless AFPM generators have been studied in [6]. Two layers non overlapping winding is considered in this study. Number of stator coils can be found from (11) as follows; [4]

$$Q_c = \frac{3}{4}2p \quad (11)$$

where p is the number of pole pairs. Number of turns per coil per phase (N_c) and the cross section area of each coil can be calculated from (12) and (13).

$$N_c = \frac{\pi a_w D_{out} A_e (1+k_d)}{4\sqrt{2} Q_c I_a} \quad (12)$$

$$s_w = \frac{2N_c I_a}{K_f a_w J_a} \quad (13)$$

where I_a, J_a, a_w and K_f are respectively, phase current, current density, number of parallel current paths and fill factor. One of the most important limitations in the winding design of these machines is the limited space to place the winding in the inner radius of the machine. For sufficient mechanical strength of stator resin disc in the inner radius of the machine, space factor (k_s) conception is used in the equations. The minimum axial length of the winding (s_d) and the axial length of the resin stator disc (L_s) can be calculated from (14) and (15). The axial increment on each side of the stator resin disc (l_s) is assumed in the computation of L_s. Regarding the practical conditions of the winding the value of l_s can be assumed between 0.2 and 1 mm, which is considered equal to 0.5 mm in this study.

$$s_d = \frac{2s_w Q_c}{k_s \pi D_{in}} \quad (14)$$

$$L_s = s_d + 2l_s \quad (15)$$

The axial length of PMs can be calculated from (16) in relation to the effective axial length of generator, PM flux leakage factor (k_{pm}) and magnetic properties of PMs [24].

$$L_{pm} = \frac{\mu_r B_g (L_s + 2g)}{2(0.95B_r - B_g / k_{pm})} \quad (16)$$

where B_r is the residual flux density of PM, g is the air gap length and μ_r is magnet permeability. The axial length of the rotor disc can be calculated by considering the appropriate value of the flux density in the rotor disc core. Also, the

mechanical restrictions, in the generators with a high number of poles should be considered in computation of the axial length of the rotor disc [25].

3.2. *Magnetic Equivalent Circuit Model*

Because of the inherent 3-D geometry of the AFPM machines, analytical analysis in the average radius does not possess adequate accuracy. Therefore, in this study, the quasi-3-D computation method [26] is used for accurate MEC modeling of the coreless AFPMSG. In the quasi-3-D computation method, the generator is disparted into several layers, which are used to develop seprate 2-D models of the machine. A 2-D model of coreless AFPMSG in the mean radius of the layer *i* is shown in Fig. 4, where the flux paths are demonstrated for one half of a pole pair. Because of the variations of flux density in the rotor yokes, the reluctance of rotor back iron is considered in two parts: the reluctance of the inter polar region ($R_{r1,i}$) and the reluctance behind the PMs ($R_{r2,i}$). The total value of rotor reluctance for a pole pitch can be defined as (17).

$$R_{r,i} = R_{r1,i} + 2R_{r2,i} \tag{17}$$

Based on model symmetry, the reduced MEC model of the *i*th layer for one magnet pole is shown in Fig. 5. $R_{g,i}$, $R_{r,i}$, $R_{pm,i}$, $R_{mr,i}$, and $R_{mm,i}$ are in order, the reluctances of the air gap, rotor back iron, magnet, magnet-to-rotor leakage flux, and magnet-to-magnet leakage flux in layer *i*. Also in Fig. 5, $\Phi_{m,i}$, $\Phi_{g,i}$, $\Phi_{mr,i}$, $\Phi_{mm,i}$, and $\Phi_{r,i}$, respectively, represent the flux leaving the magnet, air gap flux, magnet-to-rotor leakage flux, magnet-to-magnet leakage flux, and rotor back iron flux in layer *i*.

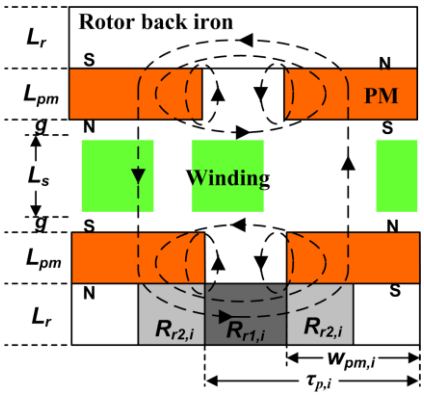

Fig. 4. Flux paths in 2-D model of the coreless AFPMSG for one half of a pole pair

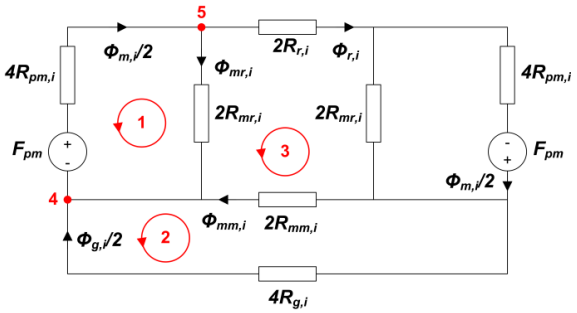

Fig. 5. MEC model of coreless AFPMSG for one half of a pole pair

The value of $R_{g,i}$ and $R_{pm,i}$ can be obtained by considering the effective air gap length and flux passing areas. The circular arc straight-line model [16] have been used for computing the leakage permeances between magnet and rotor and the leakage permeance between two magnets, which are used in calculation of $R_{mr,i}$ and $R_{mm,i}$.

As demonstrated in Fig. 4 the reluctance of rotor back iron is separated into two parts, which are calculated through the nonlinear iterative algorithm that is presented in Fig. 6. At first, the reluctances of the MEC model are developed by assigning an initial value to the relative permeability of iron parts. Then the fluxes of MEC model are determined from (18) by applying the KVL and KCL lows to the loops and nodes of MEC specified in Fig. 5.

$$\begin{bmatrix} \Phi_{m,i} \\ \Phi_{g,i} \\ \Phi_{mr,i} \\ \Phi_{mm,i} \\ \Phi_{r,i} \end{bmatrix} = \begin{bmatrix} 2R_{pm,i} & 0 & 2R_{mr,i} & 0 & 0 \\ 0 & 2R_{g,i} & 0 & -2R_{mm,i} & 0 \\ 0 & 0 & -4R_{mr,i} & 2R_{mm,i} & 2R_{r,i} \\ -0.5 & 0.5 & 1 & 1 & 0 \\ 0.5 & 0 & -1 & 0 & -1 \end{bmatrix}^{-1} \begin{bmatrix} F_{pm} \\ 0 \\ 0 \\ 0 \\ 0 \end{bmatrix} \tag{18}$$

Flux densities in the saturable parts and the new relative permeability's of the rotor iron parts are updated using B-H curve and and given in [18].

The iteration continues until the convergence condition is satisfied for all permeabilities as shown in (23) [18].

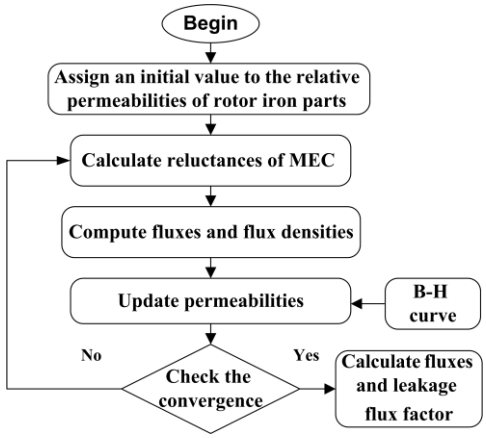

Fig. 6. The flowchart of nonlinear algorithm for consideration of rotor iron saturation

$$\left| \frac{(\mu_{f,i}^{(k)} - \mu_{f,i}^{(k-1)})}{\mu_{f,i}^{(k-1)}} \right| \le 0.01 \tag{23}$$

where $\mu_{f,i}$ is the new relative permebility of the rotor iron part and *k* is the number of iterations. After calculation of the flux distribution, PMLF factor can be obtained as the ratio of the air gap flux to the flux leaving the magnet, as follows;

$$k_{pm} = \frac{\varphi_g}{\varphi_m} = \sum_{i=1}^{N} \varphi_{g,i} \Big/ \sum_{i=1}^{N} \varphi_{m,i} \tag{24}$$

4. PSO Based Optimal Design Procedure

4.1. *Particle Swarm Optimization (PSO)*

PSO is a metaheuristic global optimization method, based on the behavior of a swarm of insects. The PSO algorithm was originally proposed by Kennedy and Eberhart in 1995 [27]. Each particle in a swarm moves through the search space using its own best found solution (personal best), and the best found solution of the swarm other particles (global best). Only two vectors are associated for each particle, position x_j and its velocity v_j. Particle positions and velocities are initialized randomly in the design space, then the algorithm operates iteratively, and the particle velocities and positions are updated, as follows;

$$v_j(t+1) = \chi[v_j(t) + c_1 r_1(t)(P_{best,j} - x_j(t)) + c_2 r_2(t)(G_{best} - x_j(t))] \quad (25)$$

$$x_j(t+1) = x_j(t) + v_j(t+1) \quad (26)$$

where $P_{best,j}$ and $G_{best,j}$ are the personal best and global best value, c_1 and c_2 are the individual and global learning rates, respectively. r_1 and r_2 are uniformly distributed random numbers in [0,1]. χ<1 is the constriction factor to reduce the velocity of particles and t is the number of iterations. During the optimization process, particle positions may be placed out of the bands. Different methods of bound handling techniques are considered in [28]. In this study, the Reflect method is used, in which the new position of the violated variables is calculated as follows;

$$\text{if } x_j(t+1) > x_{max} \text{ then } x'_j(t+1) = x_{max} - (x_j(t+1) - x_{max}) \quad (27)$$

$$\text{if } x_j(t+1) < x_{min} \text{ then } x'_j(t+1) = x_{min} + (x_{min} - x_j(t+1)) \quad (28)$$

Generally in engineering applications, accurate definition of the objective function and design restrictions is very important in the optimization procedure. Design variables are chosen in a certain range based on design knowledge and practical experience. There are four key design parameters having great influence on the generator performance, which are selected as the design variables: B_g, A_m, k_d, and α_p. Other design limitations have been discussed in the analytical design section. All the design restrictions and requirements are listed in Table 2.

The design of a 30 kW coreless AFPMSG for wind turbine application is illustrated in this study. In order to consider the generator performance over whole operating range of wind speed, the objective function is defined to design a generator with high amount of AEY, as expressed in (29) and (30).

$$f(B_g, A_m, k_d, \alpha_p) = -(P_{e,pu}) \quad (29)$$

$$P_{e,pu} = (c_{en} AEY) / P_{e,base} \quad (30)$$

where $P_{e,pu}$ is the per unit value of the annual energy profit and c_{en} is the energy price that is considered equal to 0.15 €/kWh, according to average electricity price in the world [29].

4.2. *Optimal Design Algorithm*

In order to obtain the optimal values of design variables, the optimization procedure is evaluated. At first, according to the rated speed value and considering the normal range of operating frequency for small wind generators [10], the number of pole pairs is assumed. Then, the number of coils is chosen to ensure a three phase output according to the algorithm given in [30]. For a double rotor AFPMSG, appropriate numbers of pole and coil are assumed as (24, 18), which is also result in proper rated frequency. The PSO program is then executed based on this combination. The flowchart of PSO based optimal design algorithm is shown in Fig. 7.

Table 2. Design restrictions and requirements

Parameter	Value
Rated power (P_{out})	30 (kW)
Rated speed (n_m)	200 (rpm)
Rated phase voltage (V_n)	220 (V)
Max and Min value of D_{in}/ D_{out} (k_d)	0.4, 0.75
Max and Min value of magnet width to pole pitch ratio (α_p)	0.5, 0.8
Max and Min of airgap flux density (B_g)	0.35, 0.7 (T)
Max and Min of electrical loading (A_e)	10, 50 (kA/m)
Physical air gap length (g)	1.5 (mm)
Maximum ratio of D_{out}/L_{tot}	10
Winding space factor (k_s)	0.8
NdFeB remanent (B_r)	1.23 (T)

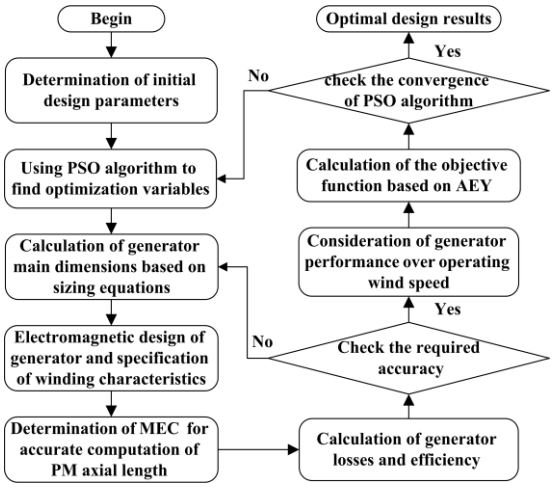

Fig. 7. Flowchart of PSO based optimal design algorithm

Generator dimensions are calculated based on sizing and electromagnetic equations, and then, the MEC model of the generator is determined for calculating the PMLF factor and axial length of the PMs. After that, the generator efficiency is obtained through the loss calculation. For considering the generator performance over whole operating wind speeds the value of output power and AEY is computed according to the wind speed distribution and turbine characteristics. The best values of the objective function and design variables are saved in each iteration of PSO algorithm.

PSO algorithm is used to perform the optimal design of coreless AFPMSG. The optimization results are achieved and presented in Table 3. In order to achieve an accurate design of the generator, further analysis is performed by 3-D FEM around the dimensions obtained via PSO.

5. Finite Element Analysis

In this section, a 3-D FE model of the coreless AFPMSG is prepared and simulated using Ansys Maxwell 16.0 software. FE analysis is performed on the generator to determine the final design parameters and validate the improved design algorithm. Further analysis in each case is performed by the 3-D FEM for minute changes in parameter values obtained via the improved design procedure. Final design dimensions are selected according to the PSO based optimization and FEM results. The final design parameters and characteristics are given in Table 4.

Table 3. Values of design variables and objective function obtained via PSO algorithm

Parameters	Value
Number of poles and coils ($2p$,Q)	(24, 18)
Ratio of inner to outer diameter (k_d)	0.627
Magnet width to pole pitch ratio (α_p)	0.79
Airgap flux density (B_g)	0.61 (T)
Electrical loading (A_e)	24277 (A/m)
Objective function value ($P_{e,pu}$)	0.849 (pu)

Table 4. Final design parameters

Parameter	Value
Rated power (P_{out})	30 (kW)
Rated speed (n_m)	200 (rpm)
Number of pole pairs (p)	12
Number of stator coils (Q_c)	18
Physical air gap length (g)	1.5 (mm)
Outer diameter (D_{out})	888 (mm)
Ratio of inner to outer diameter (k_d)	0.63
Magnet width to pole pitch ratio (α_p)	0.8
Airgap flux density (B_g)	0.61 (T)
Electrical loading (A_e)	24280 (A/m)
Axial length of PM (L_m)	20.5 (mm)
Axial length of stator (L_s)	20.7 (mm)
Number of turns per phase (N_1)	186
Efficiency at rated speed (η)	94.7%
Annual energy yield (AEY)	169.8 (MWh)

The 3-D FE model of the machine is displayed in Fig. 8 and the magnetic flux density distribution is shown in all parts of the generator. As it can be seen, the maximum value of flux density is shown in the rotor back iron core, which is equal to 1.4 T. Asymmetry of the flux distribution in the rotor disc is due to the flux density of armature reaction. In Fig. 9 the 3-D flux density in the middle plane of the effective air gap is presented for a quarter of the generator.

The three phase voltages of the generator and their harmonic contents are presented in Fig. 10 under the rated load and power factor=0.9. As it is clear from the results, the total harmonic distortion of the voltage waveform is about 4.7%, which is due to the large value of magnet width to pole pitch ratio.

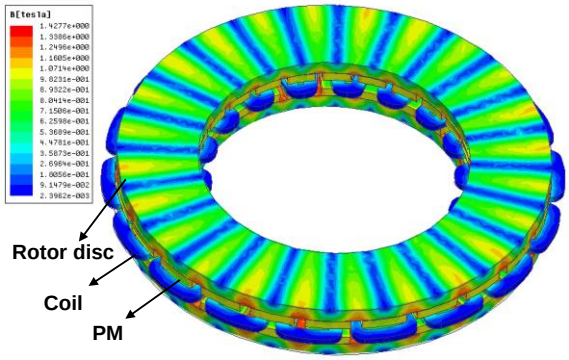

Fig. 8. Magnetic flux density distribution of the generator

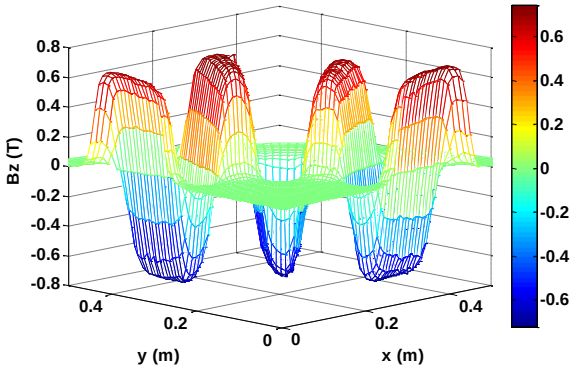

Fig. 9. 3-D flux density distribution on the middle plane of the air gap

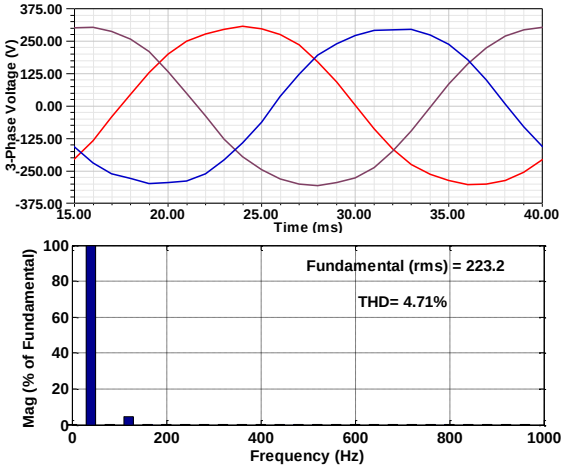

Fig. 10. Generator phase voltages waveform and harmonic content under rated load and PF=0.9

The performance of the generator with resistive-inductive load model is conducted over a range of speeds between 50 and 200 rpm. The predicted values of terminal voltage are calculated using the analytical model of the generator and compared with 3-D FEM results. Phase voltage versus load current results for different values of speed levels are shown in Figs. 11, which demonstrate excellent agreement between analytical and FEM results. As it is clear from the results, generator voltage has a linear relationship with the load current.

6. Conclusions

In this paper, a PSO based optimal design procedure of coreless AFPMSG was presented for a wind turbine application. The statistical model of wind speed distribution and wind turbine characteristic are used for considering the generator performance over the whole operating wind speed range. The objective function of the optimization is defined to design a generator with high value of AEY. A comprehensive computer aided program based on analytical design equations and MEC model of the generator is used in the design process. The reluctances of rotor back iron core are considered through a nonlinear iterative algorithm, which results in accurate design of the AFPMSG.

A 24 pole, 30 kW double rotor-one coreless stator

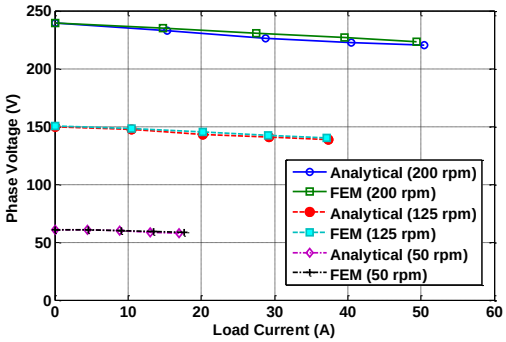

Fig. 11. Phase voltage versus load current for different speed levels

AFPMSG with concentrated winding coils was designed using the proposed procedure. The performance of the optimized generator was evaluated for different values of wind speeds and load currents. The analysis of voltage versus load current characteristics in different wind speed levels demonstrate the linear relationship even at low speed values, which make it suitable for direct-drive wind turbine application. Comparison between analytical results and 3-D FEM results illustrate the accuracy of the proposed model.

References

[1] H. Polinder, F. F. A. van der Pijl, G.-J. de Vilder, and P. J. Tavner, "Comparison of direct-drive and geared generator concepts for wind turbines " IEEE Transactions on Energy Conversion, vol. 21, no. 3, pp. 725 - 733 Sept, 2006.

[2] C. Yicheng, P. Pillay, and A. Khan, "PM wind generator topologies," IEEE Transactions on Industry Applications, DOI: 10.1109/TIA.2005.858261, vol. 41, no. 6, pp. 1619-1626, 2005.

[3] F. Giulii Capponi, G. De Donato, and F. Caricchi, "Recent Advances in Axial-Flux Permanent-Magnet Machine Technology," IEEE Transactions on Industry Applications, DOI: 10.1109/TIA.2012.2226854, vol. 48, no. 6, pp. 2190-2205, 2012.

[4] J. R. Bumby, and R. Martin, "Axial-flux permanent-magnet air-cored generator for small-scale wind turbines," IEE Proceedings - Electric Power Applications, DOI: 10.1049/ip-epa:20050094, vol. 152, no. 5, pp. 1065-1075, 2005.

[5] W. Fei, P. C. K. Luk, and K. Jinupun, "Design and analysis of high-speed coreless axial flux permanent magnet generator with circular magnets and coils," IET Electric Power Applications, DOI: 10.1049/iet-epa.2010.0081, vol. 4, no. 9, pp. 739-747, 2010.

[6] X. Bing, S. Jian-Xin, P. C. K. Luk, and F. Weizhong, "Comparative Study of Air-Cored Axial-Flux Permanent-Magnet Machines With Different Stator Winding Configurations," IEEE Transactions on Industrial Electronics, DOI: 10.1109/TIE.2014.2353012, vol. 62, no. 2, pp. 846-856, 2015.

[7] W. Rong-Jie, M. J. Kamper, K. Van der Westhuizen, and J. F. Gieras, "Optimal design of a coreless stator axial flux permanent-magnet generator," IEEE Transactions on Magnetics, DOI: 10.1109/TMAG.2004.840183, vol. 41, no. 1, pp. 55-64, 2005.

[8] T. F. Chan, and L. L. Lai, "An Axial-Flux Permanent-Magnet Synchronous Generator for a Direct-Coupled Wind-Turbine System," IEEE Transactions on Energy Conversion, DOI: 10.1109/TEC.2006.889546, vol. 22, no. 1, pp. 86-94, 2007.

[9] J. Sang-Yong, J. Hochang, H. Sung-Chin, J. Hyun-Kyo, and L. Cheol-Gyun, "Optimal Design of Direct-Driven PM Wind Generator for Maximum Annual Energy Production," IEEE Transactions on Magnetics, DOI: 10.1109/TMAG.2007.916250, vol. 44, no. 6, pp. 1062-1065, 2008.

[10] J. Faiz, B. M. Ebrahimi, M. Rajabi-Sebdani, and M. A. Khan, "Optimal design of permanent magnet synchronous generator for wind energy conversion considering annual energy input and magnet volume," in International Conference on Sustainable Power Generation and Supply, DOI: 10.1109/SUPERGEN.2009.5348100, 2009, pp. 1-6.

[11] P. Yu-Seop, J. Seok-Myeong, C. Ji-Hwan, C. Jang-Young, and Y. Dae-Joon, "Characteristic Analysis on Axial Flux Permanent Magnet Synchronous Generator Considering Wind Turbine Characteristics According to Wind Speed for Small-Scale Power Application," IEEE Transactions on Magnetics, DOI: 10.1109/TMAG.2012.2204732, vol. 48, no. 11, pp. 2937-2940, 2012.

[12] N. Rostami, M. R. Feyzi, J. Pyrhonen, A. Parviainen, and V. Behjat, "Genetic Algorithm Approach for Improved Design of a Variable Speed Axial-Flux Permanent-Magnet Synchronous Generator," IEEE Transactions on Magnetics, DOI: 10.1109/TMAG.2012.2204764, vol. 48, no. 12, pp. 4860-4865, 2012.

[13] A. Mahmoudi, S. Kahourzade, N. A. Rahim, H. W. Ping, and M. N. Uddin, "Design and prototyping of an optimised axial-flux permanent-magnet synchronous

machine," IET Electric Power Applications, DOI: 10.1049/iet-epa.2012.0377, vol. 7, no. 5, 2013.

[14] B. Xia, P. C. K. Luk, W. Fei, and L. Vu, "Particle swarm optimization of air-cored axial flux permanent magnet generator for small-scale wind power systems," in 7th IET International Conference on Power Electronics, Machines and Drives (PEMD 2014), DOI: 10.1049/cp.2014.0295, 2014, pp. 1-6.

[15] H. Chang-Chou, and Y. H. Cho, "Effects of leakage flux on magnetic fields of interior permanent magnet synchronous motors," IEEE Transactions on Magnetics, DOI: 10.1109/20.947055, vol. 37, no. 4, pp. 3021-3024, 2001.

[16] Q. Ronghai, and T. A. Lipo, "Analysis and modeling of air-gap and zigzag leakage fluxes in a surface-mounted permanent-magnet Machine," IEEE Transactions on Industry Applications, vol. 40, no. 1, pp. 121-127, 2004.

[17] M. Sadeghierad, H. Lesani, H. Monsef, and A. Darabi, "Leakage flux consideration in modeling of high speed axial flux PM generator," in IEEE International Conference on Industrial Technology (ICIT), DOI: 10.1109/ICIT.2008.4608688, 2008, pp. 1-6.

[18] S. Mohammadi, and M. Mirsalim, "Analytical Design Framework for Torque and Back-EMF Optimization, and Inductance Calculation in Double-Rotor Radial-Flux Air-Cored Permanent-Magnet Synchronous Machines," IEEE Transactions on Magnetics, DOI: 10.1109/TMAG.2013.2279129, vol. 50, no. 1, pp. 1-16, 2014.

[19] J. F. Manwell, J. G. McGowan, and A. L. Rogers, Wind Energy Explained: Theory, Design and Application, 2nd ed., UK: John Wiley & Sons, 2009.

[20] X. Yuanye, K. H. Ahmed, and B. W. Williams, "Wind Turbine Power Coefficient Analysis of a New Maximum Power Point Tracking Technique," IEEE Transactions on Industrial Electronics, DOI: 10.1109/TIE.2012.2206332, vol. 60, no. 3, pp. 1122-1132, 2013.

[21] S.M. Muyeen, Junji Tamura, and T. Murata, Stability Augmentation of a Grid-connected Wind Farm: Springer London, 2009.

[22] J. F. Gieras, R. J. Wang, and M. J. Kamper, Axial Flux Permanent Magnet Brushless Machines, 2nd ed., New York: Springer, 2008.

[23] P. R. Upadhyay, and K. R. Rajagopal, "FE Analysis and Computer-Aided Design of a Sandwiched Axial-Flux Permanent Magnet Brushless DC Motor," IEEE Transactions on Magnetics, vol. 42, no. 10, pp. 3401-3403, 2006.

[24] J. L. S. Huang, F. Leonardi, T. A. Lipo, "A Comparison of Power Density for Axial Flux Machines Based on General Purpose Sizing Equations," IEEE Transactions on Energy Conversion, vol. 14, no. 2, pp. 185-192, June, 1999.

[25] A. Parviainen, "Design of axial flux permanent magnet low speed machines and performance comparison between radial flux and axial flux machines," Phd Thesis, Lappeenranta University of Technology, Lappeenranta, Finland, 2005.

[26] A. Parviainen, M. Niemela, and J. Pyrhonen, "Modeling of axial flux permanent-magnet machines," IEEE Transactions on Industry Applications, DOI: 10.1109/TIA.2004.834086, vol. 40, no. 5, pp. 1333-1340, 2004.

[27] J. Kennedy, and R. Eberhart, "Particle swarm optimization," in IEEE International Conference on Neural Networks, 1995, pp. 1942-1948.

[28] S. Helwig, J. Branke, and S. M. Mostaghim, "Experimental Analysis of Bound Handling Techniques in Particle Swarm Optimization," IEEE Transactions on Evolutionary Computation, DOI: 10.1109/TEVC.2012.2189404, vol. 17, no. 2, pp. 259-271, 2013.

[29] Average electricity prices around the world, 2011 [Online]. Available: https://www.ovoenergy.com/guides/energy-guides/average-electricity-prices-kwh.html.

[30] M. J. Kamper, W. Rong-Jie, and F. G. Rossouw, "Analysis and Performance of Axial Flux Permanent-Magnet Machine with Air-Cored Nonoverlapping Concentrated Stator Windings," IEEE Transactions on Industry Applications, vol. 44, no. 5, pp. 1495-1504, 2008.